

FINAL REPORT

Project Title: Development of Continuous, Direct Feedback Control Systems for Sintering of Metallic Components

Covering Period: May 1, 2003 through December 31, 2004

Date of Report: September 18, 2006

Recipient: Worcester Polytechnic Institute
100 Institute Road
Worcester, MA 01609

Award Number: DE-FC36-03ID14464

Subcontractors: Oak Crest Institute of Science

Other Partners: N/A

Contact(s): Diran Apelian, Sc.D. (PI)
Howmet Professor of Mechanical Engineering
Director, Metal Processing Institute
Worcester Processing Institute, 100 Institute Road
Worcester, MA 01609
Voice: 508-831-5992. Fax: 508-831-5993
email: dapelian@wpi.edu

Marc M. Baum, Ph.D. (co-PI)
Oak Crest Institute of Science
2275 E. Foothill Blvd.
Pasadena, CA 91107
Voice: 626-817-0883. Fax: 626-817-0884
email: m.baum@oak-crest.org

Project Team: Debo Aichbhaumik, Ph.D.
Project Manager
U.S. Department Of Energy
Golden Field Office
1617 Cole Blvd.,
Golden, CO 80401-3393
Voice: 303-275-4763. Fax: 303-275-4753
email: debo.aichbhaumik@go.doe.gov

Document Availability:

Reports are available free via the U.S. Department of Energy (DOE) Information Bridge:

Web Site <http://www.osti.gov/bridge>

Reports are available to DOE employees, DOE contractors, Energy Technology Data Exchange (ETDE) representatives, and Informational Nuclear Information System (INIS) representatives from the following source:

Office of Scientific and Technical Information
P.O. Box 62
Oak Ridge, TN 37831
Tel: (865) 576-8401
Fax: (865) 576-5728
E-mail: reports@osti.gov
Web Site: <http://www.osti.gov/contact.html>

Acknowledgment: This report is based upon work supported by the U. S. Department of Energy under Award No. DE-FC36-03ID14464.

Disclaimer: Any findings, opinions, and conclusions or recommendations expressed in this report are those of the author(s) and do not necessarily reflect the views of the Department of Energy.

Proprietary Data Notice:
Not applicable

Table of Contents

	<i>Page number</i>
Document availability/Acknowledgment/Disclaimer/Proprietary data notice	2
List of Figures	4
Project Objective	5
Background	5
Body of the report	5
Accomplishments	11
Conclusions	11
Figures	12

List of Figures

- Figure 1: Mass distribution as a function of mean particle diameter for manually-mixed iron-EBS samples (red open circles) and re-powdered compact (black open squares).
- Figure 2: Experimental set-up.
- Figure 3: IR spectra of carbon monoxide (CO - red open circles), methane (CH₄ – blue open circles), and carbon dioxide (CO₂ – closed squares).
- Figure 4: Time dependence of total pressure for particles with sizes less than 53 μm at 400°C.
- Figure 5: IR spectrum of yellow product and EBS.
- Figure 6: Temperature dependence of total pressure measured after 1 h of heating and corrected for background of CO and CO₂ from the Fe-C mixture.
- Figure 7: IR spectra of the gas-phase products measured at 700°C.
- Figure 8: Temperature dependence of absorbance corresponding to hydrocarbon chains.
- Figure 9: Total pressure dependence with temperature for EBS decomposition.
- Figure 10: Breadboard gas analyzer.
- Figure 11: Schematic diagram showing the operational principle of the breadboard gas analyzer.
- Figure 12: Performance data using breadboard analyzer.

Project Objective: Development of a control system for the sintering of iron compacts

Background: *N,N*-Ethylenebisstearamide (EBS) is one of the most commonly-used lubricants in the powder metallurgy (PM) industry in the sintering process. During sintering, the lubricated powder compacts are heat-treated to temperatures in excess of 1,200 °C thus fusing adjacent particles and yielding a part with improved mechanical strength.

Delubrication commonly is achieved in the first zone of a sintering furnace by heating the part to temperatures in the 500-600 °C temperature range at a fixed rate and under controlled atmospheric conditions; this strategy minimizes defects, carbon contamination, and compact deformation. The de-lubricated part then enters the second zone (commonly in the 1200-1300 °C temperature range) for sintering. The third zone cools the sintered part at a desired rate to obtain the requisite micro-structural properties. Controlled delubrication is imperative towards achieving high quality parts for the following reasons: the elevated thermal gradient at the transition between the first and second zones can cause parts to expand rapidly and develop microscopic fissures (.blistering.); improper gas flows and belt speeds can lead to carbon deposition on the part and at the grain boundaries (sooting); delubrication products deposit throughout the furnace, even in the coolers, which are far removed from the preheating chamber, leading to significant maintenance costs; pollutants emitted in the exhaust stream of furnaces operating inefficiently are increasingly of environmental concern.

In practice, lubricant removal is difficult to control, which often leads to reduced yields in PM manufacturing processes. Throughput is another important issue: process control ideally should lead to a delubrication cycle that yields defect-free parts in a minimum of furnace time, thereby increasing productivity and reducing the net energy consumption. Efficient process control requires rapid monitoring of suitable indicators, preferably gas-phase products of delubrication. EBS thermolyzes relatively cleanly in a range of furnace atmospheres, but the mechanism governing the pyrolysis of EBS, compacted with iron powder, is not known and needs to be investigated to determine the parameters important for industrial control, as well as the optimal conditions of delubrication. In addition, a thorough understanding of the pre-sintering chemistry will enable the development of a process control sensor.

Body of the report: Year I efforts were dedicated to two main tasks: (1) investigation of the mechanism and reaction kinetics of EBS pyrolysis under vacuum conditions; and (2) design of a breadboard gas analyzer for continuous monitoring of indicator species form during EBS pyrolysis.

Task 1

In the present work, the formation of gas-phase products of EBS (Aldrich) pyrolysis was measured in the 300-700 °C temperature window. The investigated iron-EBS mixtures and repowdered compact (obtained from Pacific Sintering, Inc., compacted at 40 T-in²) contained 2 % copper, 0.75 % EBS, and carbon. The set of sieves with different mesh sizes used to fractionate particles by size afforded samples with the following size distributions, where D_p is the mean particle diameter:

- $D_p < 53 \mu\text{m}$;
- $53 \mu\text{m} < D_p < 106 \mu\text{m}$;
- $106 \mu\text{m} < D_p < 125 \mu\text{m}$;
- $125 \mu\text{m} < D_p < 180 \mu\text{m}$;
- $180 \mu\text{m} < D_p < 212 \mu\text{m}$;
- $212 \mu\text{m} < D_p < 300 \mu\text{m}$.

The mass distributions as a function of D_p recorded for manually-mixed iron-EBS samples (i.e., not compacted; red open circles) and re-powdered compact (black open squares) are presented in **Figure 1**. There is no significant difference between these samples in terms.

The experiments were carried out using the setup shown in **Figure 2**, made up of four principal components: (1) heating iron-EBS compact; (2) measuring pressure of gas phase products of EBS decomposition (Baratron); (3) freezing of volatile products of EBS decomposition using liquid N₂; (4) identifying and measuring volatile products by FTIR spectroscopy (Magna-IR 5600, Nicolet).

The sample was contained in a quartz inset. Heating of the sample was carried out by inserting the support into the tube furnace, preheated to the temperature used for the experiment. The temperature was measured near the reaction zone and was varied between 300 and 700 °C, depending on the experiment.

Sample mass was measured using a 5-decimal place analytical balance (Fisher) before and after heating. Sample mass loss over the course of an experiment (ΔM , eq. 1) was recorded for each experiment.

$$\Delta M = m_{prod} + m_{gas} \quad (1)$$

The mass of gases produced from EBS decomposition (m_{gas}) was calculated by subtraction. The mass of pyrolysis products (m_{prod}) was determined by weighting the inset after removing iron powder and subtracting weight of inset alone. Melting points (Fisher) of solid residues were recorded and are uncorrected.

The kinetics of gas-phase product formation from EBS decomposition was observed in terms of pressure growth. The

products condensed in a cool region of the setup were analyzed by FTIR absorption spectroscopy. IR Spectra of carbon monoxide (CO; red open circles), methane (CH₄; blue open circles), and carbon dioxide (CO₂; closed squares) were calibrated using 100 % cylinder gases in the 0-100 torr range; the results are presented on **Figure 3**.

Pyrolyzed samples were preheated (T = 150 °C) for 1 hr under vacuum before each experiment to minimize the amount of residual air and H₂O.

Two types of experiment typically were performed. In first set of experiments, the repowdered sample was heated in the furnace and the formation of gas-phase products was monitored as a function of pressure growth, with the rest of setup at room temperature. At the end of the experiment, the set gaseous products made up of H₂, CO, CH₄ were separated from other gases by freezing a trap using liquid N₂. In the second type of experiment, the formation of gas-phase products was monitored as a function of the pressure increase with the trap cooled with liquid N₂ throughout the experiment. After 1 hour of heating the trapped products of EBS decomposition were heated to room temperature.

The above measurements were analyzed in terms of a pressure ratio, α , as shown in eq. 2 and the measured IR spectra of products.

$$\alpha = (P_{\Sigma})_{N_2} / P_{\Sigma} \quad (2)$$

where $(P_{\Sigma})_{N_2}$ and P_{Σ} are the pressures of the gas-phase products measured under conditions when part of setup was and was not under liquid N₂, respectively, during the course of pyrolysis.

The time dependence of the total pressure growth was measured for particles with sizes below 53 μm at temperatures ranging from 300 to 700 °C, as shown in **Figure 4** at T = 400 °C.

An induction period (ca. 100 s at 400 °C) and bi-modal exponential pressure growth was observed. The induction period can be described in terms of a mechanism of EBS decomposition that includes the **indirect** formation of gas-phase products from EBS pyrolysis; i.e., by formation of gas-phase products from primary products derived from EBS decomposition. The indirect formation of gas-phase products from EBS also was supported by our temporal measurements, where the induction period is very close in magnitude to the time needed to remove EBS from the repowdered samples; 2.5 to 3.0 min at 400 °C. The induction period decreased with increasing experimental temperature.

The formation of solid residues condensed in the cold portion of setup was observed. The identity of these solid residues has not

been determined unambiguously, but it is thought that they form *via* (quasi)-simultaneous evaporation and decomposition of EBS. Two principal compounds, or compound mixtures, (yellow and white) are observed consistently following 2 min at 700 °C. The white compound was found to be similar the condensable solid formed at 400 °C. The IR spectrum of white residue (mp = 148.3 ± 0.3 °C) was found to closely resemble that of EBS (mp = 146.0 ± 0.1 °C), with the exception of peaks at 960 and 1250 cm⁻¹. The relative value of these peaks compared with the strong CH band at 2900 cm⁻¹ allowed a semiquantitative comparison of the white material to EBS. The ratio of the absorbance at 960 cm⁻¹ (A_{960}/A_{2900}) for the white product was found to be significantly greater than that measured for EBS. The peak at 1250 cm⁻¹ was only observed in an IR spectrum of EBS, although it may be hidden in the noise for the white product. Based on these observations, it was concluded that the white product consists of a mixture of EBS and a decomposition product.

The IR spectrum of yellow products (mp = 143.8 °C) is presented in **Figure 5** and is clearly different from that of EBS.

The bi-modal pressure growth shown in **Figure 4** were recorded with 1 s (for fast reaction) and 10 s (for slow reaction) time resolution and were fitted by simple first-order rate constant for $T = 300$ °C, or two-exponential growths for $T > 300$ °C. The magnitude of the observed rate constants, $k_{1\text{obs}}(T)$ for the first step of pressure increase were found to be ca. 10 times faster than those describing the second step, $k_{2\text{obs}}(T)$, of pressure growth; the values of $k_{1\text{obs}}(T) = (1.7 \pm 0.4) \times 10^{-2} \text{ s}^{-1}$ and $k_{2\text{obs}}(T) = (1.1 \pm 0.5) \times 10^{-3} \text{ s}^{-1}$ measured at $T = 773 \text{ K}$ were found to be weakly dependent on temperature. The closed values of the corresponding activation energy (E_a) in the temperature range of 400 to 700 °C have been calculated as 13 and 8 kJ mol⁻¹ for the fast and slow steps, respectively. In all experiments the increase of total pressure was found to be insignificant after 1 h of heating (i.e., pyrolysis complete).

The temperature dependence of total pressure measured after 1 h of heating and corrected for background emission of CO and CO₂ from the Fe-C mixture is presented in **Figure 6** (closed circles).

There appears to be a dependence of pressure growth on temperature up to ca. 500 °C. This temperature dependence of total pressure was found to be significantly higher than that measured when same amount of “free” EBS was heated under the same condition (open squares), implying that iron and/or carbon are required elements in the pyrolysis (*vide infra*).

The main gas phase products of EBS decomposition have been measured and identified using IR absorption spectroscopy. The spectrum of the gas-phase products measured at 700 °C is

presented in **Figure 7**, illustrating CH₄, CO, CO₂, NH₃, C₂H₄, H₂O and two types of hydrocarbons are primary products.

The formation of two different hydrocarbons was inferred on the basis of temperature dependence of absorbance corresponded to hydrocarbons chain (**Figure 8**, blue open and closed triangles). **Figure 8.**

The temperature dependence of CH₄, CO and CO₂ is presented on **Figure 9**.

The total pressure calculated using the partial pressures of these three gases (estimated from their IR absorbance) was found to be close to the total pressure measured experimentally. Based on this observation, it was concluded that CH₄, CO and CO₂ are the principal gas-phase products of EBS decomposition. However, the formation of CO₂ from stearic acid, a common contaminant of EBS, should be taken into account.

The mechanism describing the formation of gas-phase products and EBS decomposition is still under investigation. According to our preliminary results, the primary products of EBS decomposition are low-volatile compounds that subsequently decompose to afford gas-phase products. The formation of CO, CH₄, NH₃ and hydrocarbons has been attributed to the gas-phase reactions. The mechanism of CO₂ formation could be described by surface reactions, but a contribution from gas-phase reactions cannot be excluded at this point.

An effect of carbon on the formation of gas-phase products was observed and was attributed to catalysis, or mediation, of EBS decomposition. The effect of iron on EBS decomposition was found to be significantly lower than that observed for carbon. Because of high background emission of CO and CO₂ when iron powder was heated alone, it was difficult to resolve products of EBS decomposition from this background emission (i.e., effect of iron on EBS decomposition measured in the present work may be lower than that observed experimentally).

Task 2

The above investigations suggest that CO₂ and CH₄ would be useful indicators of the extent of EBS decomposition (i.e., delubrication), with the concentration of CO₂ indicating the onset of delubrication and the concentration of CH₄ indicating completion (**Fig. 9**). It appears that CO primarily is formed by reduction of iron oxide(s) by the carbon dopant and, therefore, does not represent a suitable indicator of delubrication. Our efforts in the development of a process sensor (CO/CO₂ gas analyzer) were largely guided by results indicating that CO could be a useful delubrication indicator. We in the process of converting the CO channel to a CH₄ measurement channel; both gases can be

measured using a very similar spectroscopic approach, gas filter correlation (*vide infra*). Thus, a CO/CO₂ breadboard analyzer is described here with the above caveat.

The breadboard gas analyzer (**Fig. 10**) employs IR absorption spectroscopy as its principle of operation. Light from an IR emitter is collected, modulated at 900 Hz, collimated by an off-axis parabolic reflector (OAP), projected through a sample cell containing the gas mixture to be continuously sampled from the heat treatment process, and projected into an optical head (**Fig. 11**) where the transmitted radiation is analyzed as a function of wavelength and digitized. The beam entering the optical head is split into four equal parts using a series of beamsplitters (BS) and projected to two pairs of detectors, D, with custom lenses (L) followed by optical filtration using appropriate narrow bandpass optical filters (NBOFs). The NBOFs for CO₂ measurement (**Fig. 7**) are centered on a strong, interference-free CO₂ absorption band (sample) and a band free of CO₂ absorption adjacent to the CO₂ band (reference). A signal proportional to the measured gas concentration at time *t*, ΔSR_t , is derived according to eq. 3.

$$\Delta SR_t = (S_0/R_0) - (S_t/R_t) \quad (3)$$

where S_0 and R_0 are the digital sample and reference detector signals, respectively, with zero gas flowing through the cell and S_t and R_t are the digital sample and reference detector signals, respectively, with process gas flowing through the cell.

For CO (or CH₄) measurement, both the sample and reference NBOFs are identical and are centered on a strong, interference-free CO absorption band (**Fig. 7**). The reference detector has a gas cell, GFC(1), containing 100 % CO in its field of view, whereas the sample detector has a gas cell, GFC(2), containing 100 N₂ in its field of view. A signal proportional to the measured gas concentration at time *t*, ΔSR_t , is derived according to eq. 4.

$$\Delta SR_t = [(S_0 - R_0)/(S_0 + R_0)] - [(S_t - R_t)/(S_t + R_t)] \quad (4)$$

where S_0 and R_0 are the digital sample and reference detector signals, respectively, with zero gas flowing through the cell and S_t and R_t are the digital sample and reference detector signals, respectively, with process gas flowing through the cell.

Preliminary performance data with the above breadboard analyzer are shown in **Figure 12**.

In both cases, the instrument shows excellent linearity, accuracy, and repeatability. We are very encouraged that this technology platform will provide for robust, reliable process analysis in the field.

Accomplishments:

G.A. Poskrebyshev, M. Baum, J.A. Moss, and D. Apelian, "Effect of Fe/C powder on the formation of Gas-phase products of vacuum pyrolysis of N,N'-Ethylenebisstearamide", Applied Catalysis, Under review.

G.A. Poskrebyshev, M. Baum, J.A. Moss, and D. Apelian, "Mechanism of N,N'-Ethylenebisstearamide pyrolysis and formation of CO, CO₂, CH₄, and C₂H₄ in the presence of Iron/Carbon powder under vacuum at 300°C <T<700°C, Abstr. Pap. Am. Chem. Soc., 2005, 229, U572.

The project was discontinued due to complete funding cut from DOE, and not all original objectives were achieved.

Conclusions

1. GC/MS measurements on the white and yellow residues formed at 700 °C have been carried out. In the white residue mixture multiple compounds with a molecular mass above 507 AMUs have been identified and attributed to primary products of EBS decomposition. Breakdown of the hydrocarbon chain as the primary step of EBS decomposition has been concluded on the basis of these observations.
2. Compounds with molecular weight above 259 and 287 AMUs have been observed in mass spectra of both residues.
3. Accurate IR spectra of the above solid mixtures have been measured. The presence of secondary, acyclic amides with shorter hydrocarbon chains has been observed for both sample groups. The presence of stearic acid and stearamide in these residues was not observed. However, formation of stearamide cannot be excluded because of rapid decomposition to ammonia, CO, and alkenes.
4. The gas phase decomposition products from an authentic sample of stearamide at 700 °C have been measured by FTIR absorption spectroscopy. The IR spectrum of the decomposition products in the 900 to 1000 cm⁻¹ range was similar to those measured for EBS at temperatures above 500 °C and attributed to NH₃ formation.
5. The formation of CO, NH₃ and/or C₂H₄, and, partially, CH₄ has been attributed to gas phase pyrolysis of secondary products of EBS decomposition.
6. Formation of methane *via* the decomposition of primary products also has been observed and the direct formation of small amounts on the surface of the iron powder cannot be ruled out.
7. Formation of CO₂ has been mainly attributed to direct decomposition of EBS and stearic acid (contamination of EBS) but the partial formation of CO₂ in secondary reaction cannot be excluded.

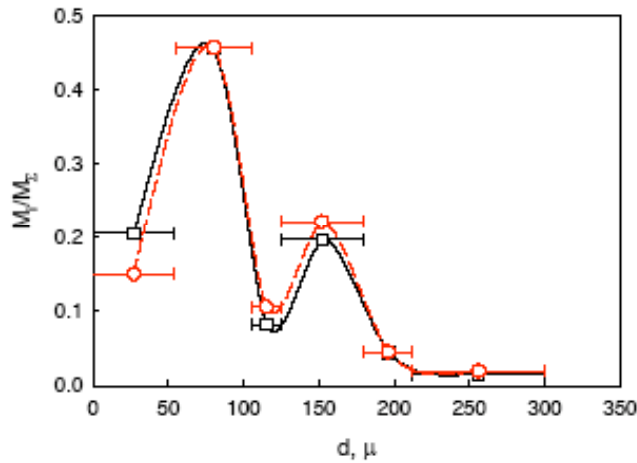


Figure 1: Mass distribution as a function of mean particle diameter for manually-mixed iron-EBS samples (red open circles) and re-powdered compact (black open squares).

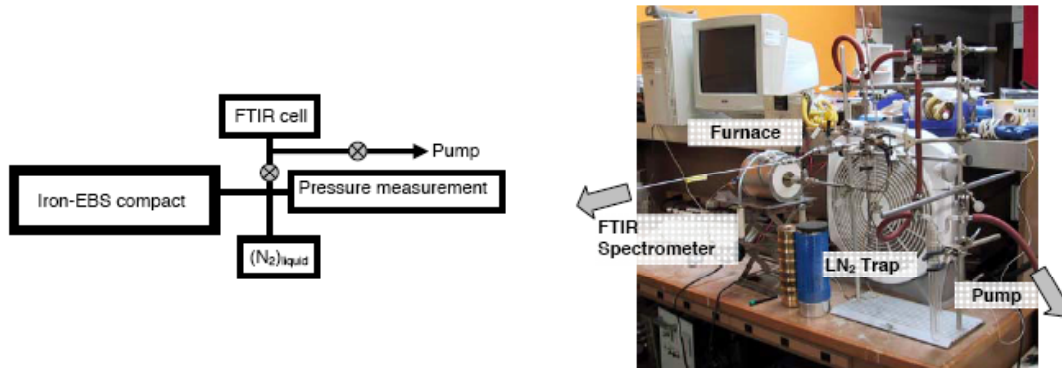


Figure 2: Experimental set-up.

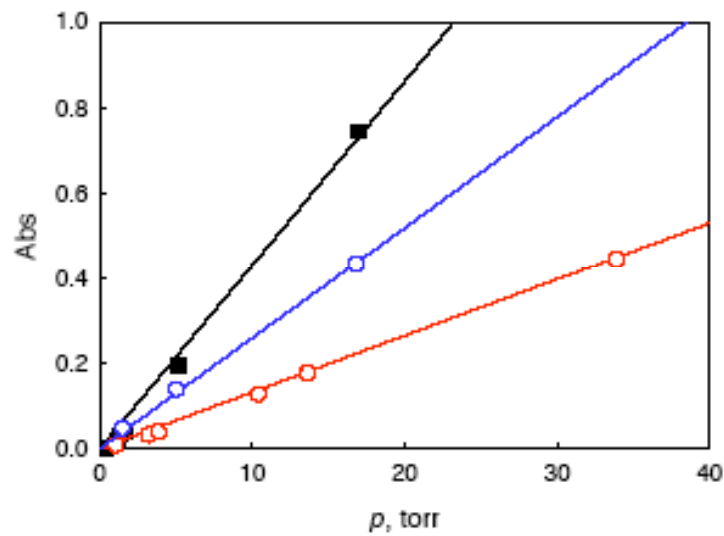


Figure 3: IR spectra of carbon monoxide (CO - red open circles), methane (CH₄ - blue open circles), and carbon dioxide (CO₂ - closed squares).

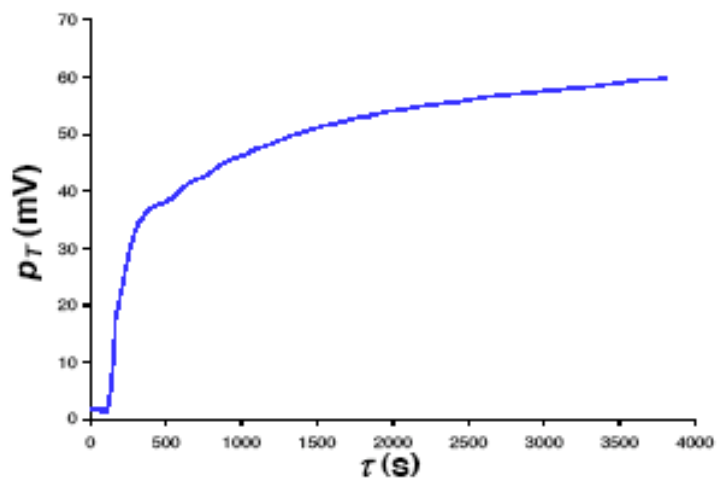


Figure 4: Time dependence of total pressure for particles with sizes less than 53 μm at 400°C.

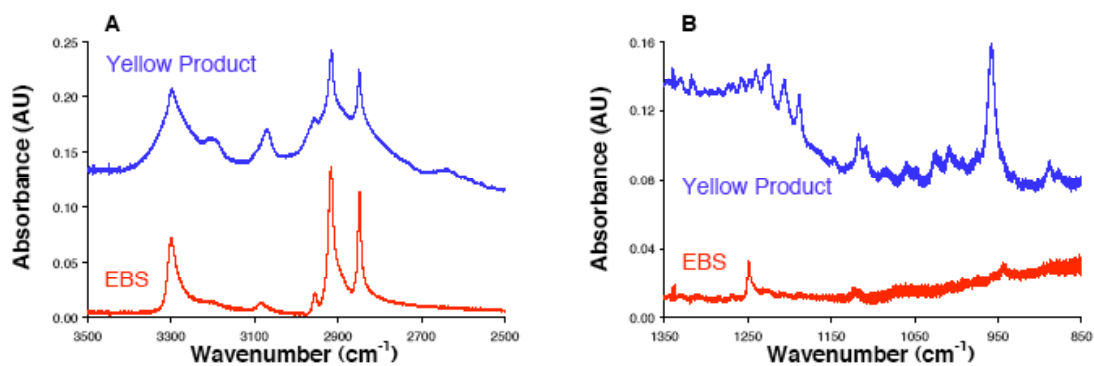


Figure 5: IR spectrum of yellow product and EBS.

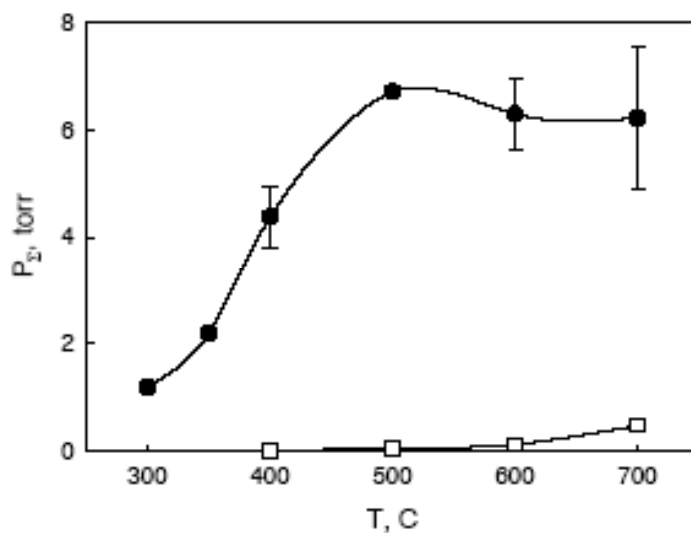


Figure 6: Temperature dependence of total pressure measured after 1 h of heating and corrected for background of CO and CO₂ from the Fe-C mixture.

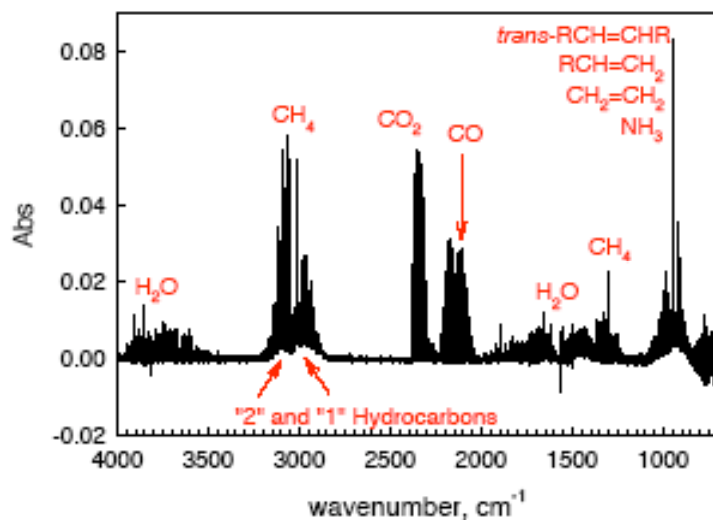


Figure 7: IR spectra of the gas-phase products measured at 700°C.

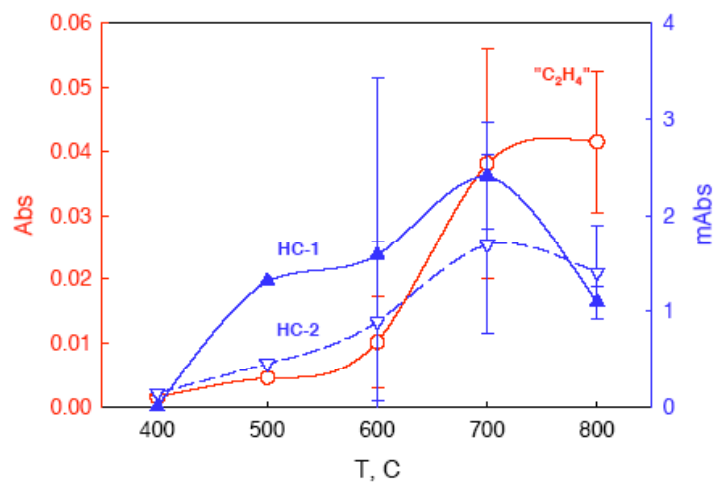


Figure 8: Temperature dependence of absorbance corresponding to hydrocarbon chains.

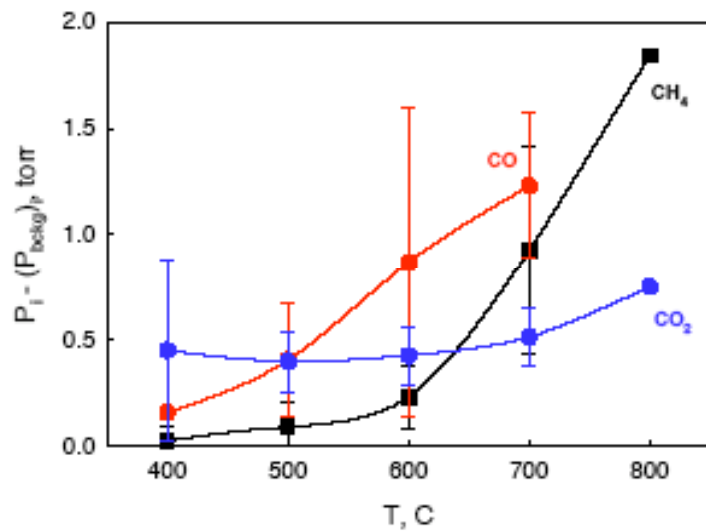


Figure 9: Total pressure dependence with temperature for EBS decomposition.

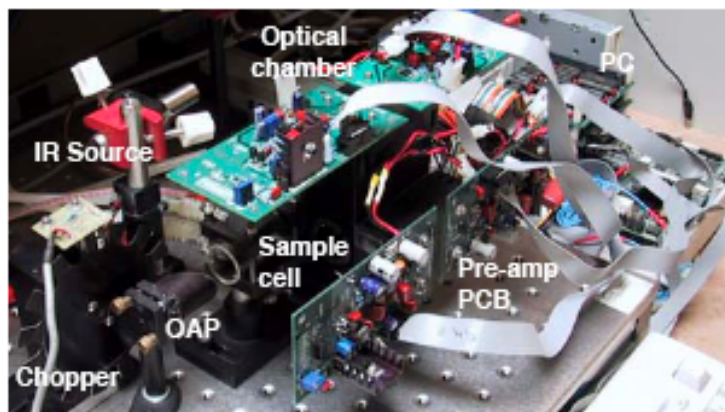


Figure 10: Breadboard gas analyzer.

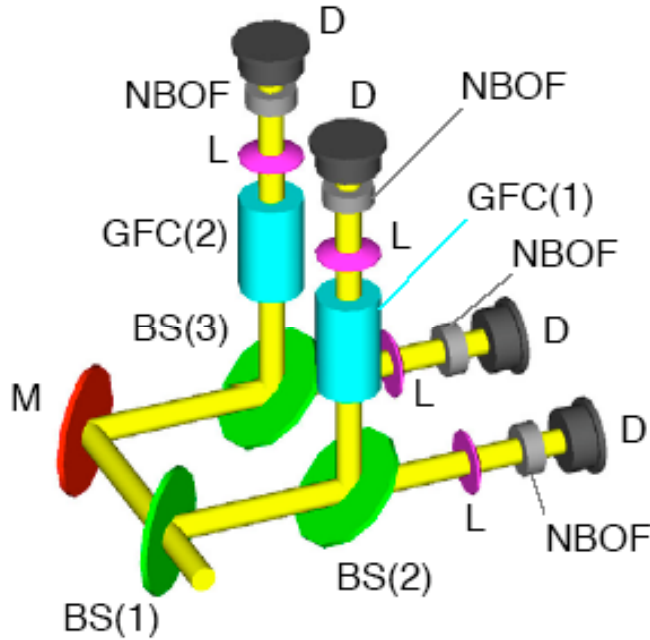


Figure 11: Schematic diagram showing the operational principle of the breadboard gas analyzer.

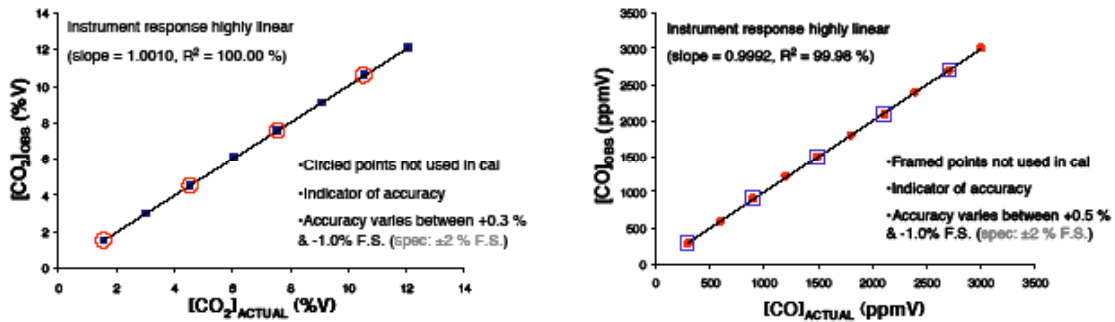


Figure 12: Performance data using breadboard analyzer.